Direct Observational Evidence of Altered Mesosphere Lower Thermosphere Mean Circulation from a Major Sudden Stratospheric Warming

Federico Gasperini[1], McArthur Jones Jr[2], Brian J. Harding[3], Thomas J. Immel[3]

[1]Orion Space Solutions, 282 Century Pl #1000, Louisville, CO, USA
[2]Space Science Division, U.S. Naval Research Laboratory, Washington, DC, USA
[3]Space Sciences Laboratory, University of California, Berkeley, CA, USA

Key Points:

- A prominent (∼30 m/s) reversal in the MLT mean meridional circulation during the January 2021 major SSW is observed in MIGHTI winds
- Strong (∼35 m/s) MLT westward flow enhancements are observed following the onset of the SSW
- Amplification in MLT SW2 zonal wind amplitudes are consistent with the observed westward flow enhancements

Corresponding author: Federico Gasperini, federico.gasperini@orionspace.com

Abstract

Sudden stratospheric warmings (SSWs) are large-scale phenomena characterized by dramatic dynamic disruptions in the stratospheric winter polar regions. Previous studies, especially those employing whole atmosphere models, indicate that SSWs have strong impacts on the circulation of the mesosphere lower thermosphere (MLT) and drive a reversal in the mean meridional circulation (MMC) near 90-125 km altitude. However, the robustness of these effects and the roles of SSW-induced changes in global-scale wave activity to drive the reversal have been difficult to observe simultaneously. This work employs horizontal lower thermospheric (∼93-106 km altitude) winds near 10°S-40°N latitude from the Michelson Interferometer for Global High-resolution Thermospheric Imaging (MIGHTI) instrument onboard the Ionospheric Connection Explorer (ICON) to present observational evidence of a prominent MLT MMC reversal associated with the January 2021 major SSW event and to demonstrate connections to semidiurnal tidal activity and possible associations with a ∼3-day ultra-fast Kevin wave (UFKW).

Plain Language Summary

The winds in the mesosphere lower thermosphere (MLT) are strongly impacted by dramatic changes in the stratospheric winter polar regions associated with Sudden Stratospheric Warmings (SSWs). Models have shown that the climatological direction of the MLT north-south and vertical circulation, characterized by equatorward flow near ∼100-120 km and poleward flow near ∼80-100 km, reverses following the onset of SSWs. Yet, the impacts and causes of these dynamical effects are not well established observationally due to the lack of comprehensive global measurements of the MLT region. This study evaluates the evolution of MLT winds and associated tidal and ultra-fast Kevin wave (UFKW) variations during the January 2021 SSW using horizontal wind observations from the Michelson Interferometer for Global High-resolution Thermospheric Imaging (MIGHTI) instrument onboard the Ionospheric Connection Explorer (ICON) to present observational evidence of a large MLT north-south wind reversal due to the SSW and associated global-scale wave influences.

1 Introduction

Stratospheric Sudden Warmings (SSWs) are global-scale meteorological events driven by the dissipation of vertically-propagating planetary waves originating in the troposphere

(Matsuno, 1971; Butler et al., 2015). SSW events are characterized based on the changes that occur in the stratosphere, including a rapid increase in polar temperatures and deceleration of the zonal mean zonal winds. A SSW is classified as a major SSW if the zonal mean zonal winds at 60°N and 10 hPa reverse from eastward to westward (e.g., Charlton and Polvani, 2007). SSWs lead to significant disturbances in the whole atmosphere (Stening 1977), producing remarkable changes in composition, dynamics, and electrodynamics of the whole ionosphere-thermosphere system, pole-to-pole, as demonstrated by a number of modeling and observational studies (e.g., Goncharenko and Zhang 2008; Chau et al. 2009; Goncharenko et al. 2010; Chau et al., 2012, 2015; Butler et al., 2015; Zulicke et al., 2018; Laskar et al., 2019; Pedatella et al., 2014, 2016, 2018, 2022; Jones et al., 2020; Oberheide et al., 2020; Oberheide 2022; Siddiqui et al., 2022; Liu et al., 2022). Modeling and observational evidence also suggest that SSW impacts can extend into the summer mesosphere and mesopause region through inter-hemispheric coupling (e.g., Becker and Fritts, 2006; Tan et al., 2012; Liu et al., 2013, 2014; Miyoshi et al. 2015; Lieberman et al., 2021; Goncharenko et al., 2022). Thus, SSWs provide an exemplary case to study the coupling between the lower atmosphere and the overlying atmospheric regions.

It is now well established that the deceleration and reversal of winter stratospheric wind associated with SSWs produce significant changes in the propagation conditions of global-scale waves that lead to strong changes in upper atmospheric circulation (e.g., Liu and Roble, 2002; Tan et al., 2012; Yiğit and Medvedev, 2012, 2016; Yuan et al., 2012; Yiğit et al., 2014, 2016; Miyoshi et al., 2015; Liu, 2017; Jones et al., 2020). These SSW-induced wind and temperature disturbances in the stratosphere and mesosphere lead to enhancements in the solar semidiurnal migrating tide (SW2, 12-hour period and westward zonal wave number s = 2) and other non-migrating tidal components (e.g, Chang et al., 2009; Liu et al., 2010; Pancheva et al., 2009; Pedatella et al., 2012; Pedatella and Liu, 2013) due to nonlinear interactions with stationary planetary waves (e.g., Liu et al. 2010; Sathishkumar and Sridharan, 2013), changes in the tidal propagation conditions (e.g., Jin et al. 2012) and stratospheric ozone distribution (e.g., Goncharenko et al. 2012; Siddiqui et al. 2019). SSWs can also lead to resonant amplification of the lunar semidiurnal migrating tide (M2, 12.42-hour period) because of the atmospheric Pekeris mode (Forbes and Zhang, 2012; Liu et al., 2022). Modeling evidence (e.g., Yamazaki et al., 2020) also suggests that ultra-fast Kevin waves (UFKWs) may be amplified during SSWs, how-

ever, the relationship between SSWs and UFKWs remains unclear (e.g., England et al., 2012; Liu et al., 2012; Phanikumar et al., 2014; Sassi et al., 2013, Yamazaki et al., 2020).

Previous modeling studies (e.g., Miyoshi et al., 2015; Zhang J. et al., 2021, 2022; Orsolini et al., 2022; Wang et al., 2022) suggest that the climatological direction of the mesosphere-lower thermosphere (MLT) mean meridional circulation (MMC), characterized by upwelling in the middle winter latitudes, equatorward flow near ∼100-120 km, and poleward flow near ∼80-100 km, reverses following the onset of SSWs. Ground-to-topside model of Atmosphere and Ionosphere for Aeronomy (GAIA) model simulations from Miyoshi et al. (2015) revealed that MMC reversed in the lower thermosphere. More recently, Orsolini et al. (2022) used the Whole Atmosphere Community Climate Model with thermosphere and ionosphere eXtension (WACCM-X) in the specified dynamics configuration to show that the lower thermospheric mean meridional circulation reverses for about 10 days following the onset of elevated stratopause events in the northern hemisphere largely driven by westward-propagating planetary waves. Important impacts on MLT mean circulation have also been reported observationally (e.g., Oberheide, 2022) including enhancements of both eastward and westward directed flow associated with wave dissipation. Zhang R. et al. (2022) used Ionospheric Connection Explorer (ICON) Michelson Interferometer for Global High-resolution Thermospheric Imaging (MIGHTI) and Ion Velocity Meter (IVM) data to investigate ionosphere-thermosphere coupling during the January 2021 SSW, suggesting the importance of the F-region northward wind changes in driving anomalous ionospheric field-aligned flows. However, no studies have investigated the lower-altitude wind patterns which are thought to dominate the ionospheric SSW response.

This study examines zonal and meridional MLT (∼93-106 km) wind observations from the MIGHTI instrument onboard ICON to present observational evidence of a prominent MLT MMC reversal associated with the January 2021 major SSW event and to demonstrate connections to semidiurnal tidal activity and possible impacts on a ∼3-day UFKW with s = -1 (hereafter, UFKW1). After a brief description of the data and methods (Section 2), we show impacts on MLT dynamics and connections to wave drivers (Section 3), and provide the conclusions (Section 4).

2 ICON MIGHTI Neutral Wind Profiles and Wave Diagnostics

ICON is a NASA Heliophysics System Observatory (HSO) mission launched on 10 October 2019 into a nearly circular ∼590 km altitude and ∼27° inclination orbit to study the connections between the dynamics of the neutral atmosphere near 90-300 km and the electrodynamics of the low-latitude ionosphere (Immel et al., 2018; Immel and Eastes, 2019; Immel et al., 2021). ICON retrieves neutral wind profiles in the upper atmosphere using the Michelson Interferometer for Global High-resolution Thermospheric Imaging (MIGHTI) instrument from remote observations of green ∼557.7 nm and red ∼630.0 nm airglow emissions (Harlander et al. 2017). This work employs zonal and meridional neutral winds (ICON data product L2.2 V04) from ∼93 km to ∼106 km altitude, where continuous day and night observations are available in the 10°S to 40°N latitude range. More information on MIGHTI wind, error analyses, and validation can be found in Englert et al. (2017), Harding et al. (2017, 2021), and Makela et al. (2021). Recently, Yiğit et al (2022) examined the climatology of MIGHTI mean zonal and meridional winds and associated mean circulation finding the prevalence of eastward zonal winds and northward meridional winds and general agreement with middle thermospheric wind climatologies, validating the use of MIGHTI to study mean winds.

Based on the occurrence of occasional gaps, data quality issues, and instrument calibrations, MIGHTI allows for stable extraction of solar tides within 41-day moving windows (Cullens et al., 2020; Forbes et al., 2022). In this work, semidiurnal tidal fits are performed using 41-day moving windows on winds averaged in 6° latitude, 60° longitude, and 2-hour UT bins extending from 10°S to 40°N using the native ∼2.5 km altitude sampling. This binning effectively removes the effects of small-scale variations and improves the statistics while also leading to smoother visual depictions. Wind data flagged as bad (quality flag = 0) are not included. Many of the 0-flagged data are connected with South Atlantic Anomaly contamination. Their removal leaves gaps near 270°-330°longitude in the Southern Hemisphere that are not significantly affecting the latitude regions of primary interest for this study. Forbes et al. (2022) provide more details on the tidal diagnostics of the composite data, which closely follows the procedure adopted by Gasperini et al. (2021) in the analyses of ICON IVM data and by Gasperini et al. (2015, 2017, 2018, 2020) in the analysis of Thermosphere, Ionosphere, Mesosphere, Energetics and Dynamics (TIMED) observations. After the exact UFKW1 period is determined using spectral analysis, simultaneous least-squares fits are performed on these 41-day windows to de-

Figure 1. (a) MERRA-2 zonal and diurnal average zonal wind near 60°N latitude during 1 December 2020 - 31 January 2021. (b) Same as (a), but for MERRA-2 temperature averaged 60°N-90°N latitude. (c) Time series of (a) at 10 hPa. (d) Time series of F10.7 (black line) and Kp (blue line, left y-axis) for the same period as (a)-(c). The orange vertical lines indicate 3 January 2021 when the zonal mean zonal winds at 60°N and 10 hPa first reversed from eastward to westward.

rive SW2 and UFKW1 amplitudes and phases. UFKW1 amplitudes are extracted using 41-day moving windows for consistency with the tidal diagnostics. Daily ZM winds are obtained from ICON MIGHTI as the average from the measurements at the ascending and descending nodes. As noted by Gasperini et al. (2020) who applied a similar method to Gravity Field and Steady-State Ocean Circulation Explorer (GOCE) data, the ascending and descending ZM mean winds include both the true ZM and a contribution from SW2, which is sampled at the same phase on both orbit nodes. Along with aliasing from SW2, these ZM estimates may also be affected by LT precession, especially near the terminators.

3 Results

Figure 1 shows the height-time structure of the longitude and diurnal mean zonal wind at 60°N (panel a) and 60°-90°N polar cap temperature (panel b), the time series of the zonal mean zonal wind at 10 hPa (panel c) and the time series of the solar and geomagnetic indices (panel d) for 1 December 2020 - 31 January 2021. A major SSW event, indicated by a reversal of the 60°N stratospheric zonal mean zonal winds, started on 3 January 2021, with westward winds that persisted through 21 January (with a 2-day eastward interruption). The relatively long persistence of westward wind during this SSW was explained as a reflection of persistent strong dynamical forcing overtaking non-adiabatic cooling effects (e.g., Lu et al., 2021). More information on the lower and middle atmospheric response to this SSW can be found in the recent work by Rao et al. (2021). The geomagnetic Kp index (blue line in Figure 1d) exhibits periods of moderate activ-

Figure 2. MIGHTI longitude-mean day/night averaged meridional winds near 106 km (a) and 93 km (b) during 1 December 2020 - 31 January 2021. (a′)-(b′) Same as (a)-(b), but for zonal winds. MIGHTI meridional mean winds as a function of altitude (∼94-106 km) and latitude (∼0-40°N) during 7 December - 2 January (c) and 3-29 January (c′). (c′′) Difference between (c′) and (c). (d)-(d′′) Same as (c)-(c′′), but for zonal winds. The orange vertical lines in (a)-(a′) and (b)-(b′) indicate 3 January 2021 when the zonal mean zonal winds at 60°N and 10 hPa first reversed from eastward to westward.

ity, with values exceeding 4 on six occasions during 1 December - 31 January. The F10.7 solar flux index (black line in Figure 1d) decreases from a maximum near 110 sfu on December 1 to near 80 sfu on December 7, remaining relatively constant through January 31. It is important to note that the recurrent moderate geomagnetic activity present during this 62-day period is unlikely to generate variability at MLT heights that would significantly alias into the dynamic response to the SSW, especially considering that its day-to-day variability is very different than the timescale of the SSW (see the discussion in Oberheide (2022)).

Next, the dynamic response of the MLT to the SSW is examined by employing longitude- and day/night-averaged (hereafter, 'zonal mean') MIGHTI wind observations between ∼93 km and ∼106 km. Figure 2 shows the temporal evolution of zonal mean MIGHTI meridional (panels a and b) and zonal (panels a' and b') winds as a function of latitude (10°S-35°N) during 1 December 2020 - 31 January 2021 near 106 km and 93 km, respectively. After removing seasonal and longer-term effects by generating residuals from 27-day running means, the winds are then averaged between Dec 7 - Jan 2 ('Before SSW') and Jan 3 - Jan 29 ('During SSW'), and their altitude (∼94-106 km) and latitude (∼0-40°N) structure is illustrated in Figures 2c-2c' (Figures 2d-d') for the meridional (zonal) components. To best highlight changes associated with the SSW, Figure 2c'' (Figure 2d'') shows the differences between the 'During SSW' and the 'Before SSW' case for the meridional (zonal) wind component. As visible by close inspection of Figures 2a-2b and best

Figure 3. ICON/MIGHTI mean zonal winds near 93 km (a), MIGHTI 41-day mean zonal wind SW2 (b), SW1 (c), SW3 (d), and UFKW1 (e) amplitudes near 93 km during 1 Dec 2020 - 31 Jan 2021. (a′)-(e′) Same as (a)-(d), but near 106 km. The orange vertical lines indicate 3 January 2021 when the zonal mean zonal winds at 60°N and 10 hPa first reversed from eastward to westward.

illustrated by Figure 2c'', the meridional mean winds are found to experience a marked change in direction from primarily southward before the SSW to primarily northward during the SSW at the upper heights (i.e., above ∼98 km) and from mainly northward before the SSW to mainly southward during the SSW at the lower MLT heights (i.e., ∼95-98 km). These effects are particularly prominent near 20°N-40°N with meridional wind variations around 10-40 m/s (depending on latitude and altitude). The direction and magnitude of these wind variations provide observational confirmation of previous modeling results (e.g., Miyoshi et al., 2015) and are consistent with the understanding that the typical summer-to-winter MLT flow can be broken down during SSWs, resulting in a two-cell pattern with equatorward motion at lower heights (i.e., <90-95 km) and poleward motion aloft (i.e., >105-110 km).

Prominent enhancements in the westward mean winds following the onset of the SSW are found, with variations up to ∼35 m/s compared to the 'Before SSW' case as demonstrated by Figure 2d''. These effects exhibit a strong dependency in latitude and some in altitude, with the westward enhancements strongest at the northernmost latitudes sampled by MIGHTI (i.e., ∼30°N-40°N). Further, previous modeling work by Miyoshi et al. (2015), Oberheide et al. (2020), and Jones et al. (2020) indicate that these enhanced westward winds observed by MIGHTI are likely driven by periodic westward forcing via the Eliassen-Palm flux divergence, which then contributes to the observed residual MMC in Figure 2.

Finally, the response of MLT zonal wind wave amplitudes to the SSW is examined using 41-day running averages of MIGHTI observations. While a 35-day averaging may

be sufficient to extract the complete tidal spectrum from MIGHTI data (e.g., Cullens et al., 2020), we find that a 41-day averaging provides improved fits for latitudes above ∼25°N (see also discussion in Section 2). Figure 3 shows MIGHTI mean zonal winds near 93 km (panel a) and 106 km (panel a') and SW2, SW1, and SW3 zonal wind tidal amplitudes near 93 km (panels b-d) and near 106 km (panels b'-d'). Large enhancements in SW2 zonal wind amplitudes near 93 km and 10°N-35°N occur around 10-20 January concurrent with the significant strengthening in westward mean winds that follows the onset of the SSW. A weaker increase in SW2 amplitudes (and enhanced westward mean winds) also appears near the equator during 1-7 January. Similar to the SW2 MIGHTI wind diagnostics in Oberheide (2022), SW2 displays strong enhancements associated with the SSW near 106 km. SW1, SW2, and SW3 typically attain their largest amplitudes at mid-to-high latitudes, outside of the latitudes observed by ICON. However, recent work by Pedatella (2022) shows that simulated SD-WACCM-X SW2 amplitudes near 110 km are also strongly enhanced between 1-8 January near 50°N-60°N and 50°S-60°S, with SD-WACCM-X SW1 and SW3 zonal wind amplitudes also slightly enhanced but exhibiting more day-to-day variability. Also, note that while SSW-induced effects on SW1 and SW3 seem less prominent than those observed on SW2, it is important to keep in mind that day-to-day variability in these tidal components is largely removed by the 41-day averaging.

In addition to the semidiurnal tidal impacts previously noted, evidence of a large (∼15 m/s near 106 km) ∼3-day UFKW1 is found during this 62-day period extending from 1 December 2020 to 31 January 2021. Figures 2e-2e' show the latitude-temporal structure of its amplitudes during 1 December - 31 January near 93 km and 106 km, respectively. Enhanced UFKW1 amplitudes near 106 km observed during 11-21 January and ∼0-10°N closely resemble the SW2 amplifications found near 93 km. Connections between SSWs and UFKWs are not unexpected, as enhanced westward mean winds in the middle atmosphere would tend to favor the vertical propagation of UFKWs into the MLT given their eastward-propagation characteristics. It is well known both numerically and observationally (e.g., Forbes, 2000, 2020; Gasperini et al., 2015, 2018, 2020) that background zonal-mean zonal winds can Doppler-shift UFKWs modifying their propagation (e.g., Ekanayake et al., 1997), and thus changing their vertical wavelength (e.g., Forbes and Vincent, 1989) and susceptibility to dissipation. While of certain interest, it would

be beyond the scope of this study to investigate SSW-UFKW connections in further detail and this effort is left as an avenue for possible follow on work.

4 Summary and Conclusions

Previous whole atmosphere modeling studies suggest that the climatological direction of the MLT mean meridional circulation, characterized by equatorward flow near ∼100-120 km and poleward flow near ∼80-100 km, reverses in response to a major SSW event. However, the veracity of these modeling predictions, the robustness of the effects, and the roles of SSW-induced changes in global-scale activity to drive the reversal have yet to be observed concurrently.

This work employed zonal and meridional MLT wind observations from the MIGHTI instrument onboard ICON in the ∼93-106 km altitude range to present first-time (to the best of the authors' knowledge) observational evidence of a prominent MLT MMC reversal associated with the January 2021 major SSW event. The meridional mean winds are found to change in direction from southward before the SSW to northward during the SSW at the upper heights (i.e., above ∼98 km) and from northward before the SSW to southward during the SSW at the lower MLT heights (i.e., ∼95-98 km). These large changes in the mean meridional winds are of the order of ±30 m/s and are most prominent at the northernmost latitudes sampled by MIGHTI (i.e., 30-40°N). These wind changes provide observational confirmation of previous modeling results (e.g., Miyoshi et al., 2015) suggesting that the typical summer-to-winter MLT flow is broken down during SSWs and a resulting two-cell pattern emerges with equatorward motion at lower heights and poleward motion aloft.

Prominent enhancements (upward of ∼35 m/s) in westward mean winds are also found in response to the SSW, with effects that are strongest at higher altitudes (i.e., >102 km) and latitudes (i.e., ∼30°-40°N). Large enhancements in SW2 zonal wind amplitudes near 93 km and 10°N-35°N occurring around 10-20 January are concurrent and nearly colocated with significant strengthening in westward mean winds following the onset of the SSW. Effects associated with SW1 and SW3 are found to play a smaller role, in contrast with the discussion by Zhang R. et al (2022). Spectral analyses also reveal the presence of a ∼3-day UFKW1 with enhanced amplitudes (∼15 m/s) near 106 km occurring during 10-20 January and 0-10°N that closely resemble the SW2 amplifications

near 93 km. The latter result supports a possible connection between SSWs and UFKWs that warrants further investigation.

5 Open Research

MIGHTI ICON V04 winds were obtained from `https://icon.ssl.berkeley.edu/Data/`. Note that preliminary analyses of the recently-released MIGHTI V05 wind product support the main conclusions of this study. The 3-hourly Kp index was obtained from GFZ Potsdam at `https://kp.gfz-potsdam.de/app/files/Kp_ap_since_1932.txt`, the F10.7 cm radio flux from NASA/GSFC OMNIWeb at `https://omniweb.gsfc.nasa.gov/form/dx1.html`, and the MERRA-2 zonal wind and temperature from NASA/GSFC Global Modeling and Assimilation Office (GMAO) at `https://gmao.gsfc.nasa.gov/reanalysis/MERRA-2/data_access/`.

Acknowledgments

ICON is supported by NASA's Explorers Program through contracts NNG12FA45C and NNG12FA42I. FG acknowledges support from NASA Grant No. 80NSSC22K0019 and NSF Award No. 2113411. MJ acknowledges support from the NASA Early Career Investigator (NNH18ZDA001N-ECIP/18-ECIP_2-0018) and GOLD-ICON Guest Investigators (NNH20ZDA001N-GIGI/20-GIGI20_2-0009) programs.

References

Becker, E., and D. C. Fritts, 2006: Enhanced gravity-wave ac- tivity and interhemispheric coupling during the macwave/ midas northern summer program 2002. Ann. Geophys., 24, 1175-1188.

Butler, A. H., Seidel, D. J., Hardiman, S. C., Butchart, N., Birner, T., and Match, A. (2015). Defining Sudden Stratospheric Warmings. Bulletin of the American Meteorological Society, 96(11), 1913-1928, doi:10.1175/bams-d-13- 00173.1

Chang, L. C., Palo, S. E., and Liu, H.-L. (2009). Short-term variation of the s =1 nonmigrating semidiurnal tide during the 2002 stratospheric sudden warming. Journal of Geophysical Research, 114, D03109, doi:10.1029/2008JD010886

Charlton, A.J.; Polvani, L.M. A New Look at Stratospheric Sudden Warmings. Part I: Climatology and Modeling Benchmarks. J.Clim. 2007, 20, 449-469.

Chau, J.L.; Fejer, B.G.; Goncharenko, L.P. Quiet variability of equatorial E × B drifts during a sudden stratospheric warming event, Geophys. Res. Lett. 2009, 36, L05101.

Chau, J.-L., Goncharenko, L.-P., Fejer, B.-G., and Liu, H. L. (2012), Equatorial and low latitude ionospheric effects during sudden stratospheric warming events. Space Science Reviews, 168, 385-417, doi:10.1007/s11214-011-9797-5

Chau, J.-L., Hoffmann, P., Pedatella, N.-M., Matthias, V., and Stober, G. (2015), Upper mesospheric lunar tides over middle and high latitudes during sudden stratospheric warming events, Journal of Geophysical Research: Space Physics, 120, 3084-3096,doi:10.1002/ 2015ja020998

Cullens, C.Y., Immel, T.J., Triplett, C.C. et al. (2020), Sensitivity study for ICON tidal analysis, Prog Earth Planet Sci, 7, 18, doi:10.1186/s40645-020-00330-6

Ekanayake, E.M.P., Aso, T., & S. Miyahara (1997), Background wind effect on propagation of nonmigrating diurnal tides in the middle atmosphere, J. Atmos. Solar-Terr. Phys., 59, 401-429.

England, S. L., Liu, G., Zhou, Q., Immel, T. J., Kumar, K. K., & Ramkumar, G. (2012), On the signature of the quasi-3-day wave in the thermosphere during the January 2010 URSI World Day Campaign, Journal of Geophysical Research, 117, A06304, doi:10.1029/2012JA017558

Englert, C. R., Harlander, J. M., Brown, C. M., Marr, K. D., Miller, I. J., Stump, J. E., et al. (2017), Michelson interferometer for global high-resolution thermospheric imaging (MIGHTI): Instrument design and calibration, Space Science Reviews, 212(1-2), 553-584, doi:10.1007/s11214-017-0358-4

Forbes, J.M. (2000), Wave coupling between the lower and upper atmosphere: Case study of an ultra-fast kelvin wave, J. Atmos. Sol. Terr. Phys., 62, 1603-1621.

Forbes, J.M., Vincent, R.A. (1989), Effects of mean winds and dissipation on the diurnal propagating tide: an analytic approach, Planet, Space Sci. 37, 197-209.

Forbes, J. M., and Zhang, X. (2012), Lunar tide amplification during the January 2009 stratosphere warming event: Observations and theory, Journal of Geophysical Research, 117(A12), doi:10.1029/2012JA017963

Forbes, J. M., Maute, A., & Zhang, X. (2020), Dynamics and electrodynamics of an ultra-fast Kelvin wave (UFKW) packet in the ionosphere-thermosphere (IT), Journal of Geophysical Research: Space Physics, 125, e2020JA027856,

doi:10.1029/2020JA027856

Forbes, J. M., Oberheide, J., Zhang, X., Cullens, C., Englert, C. R., Harding, B. J., et al. (2022), Vertical coupling by solar semidiurnal tides in the thermosphere from ICON/MIGHTI measurements, Journal of Geophysical Research: Space Physics, 127, doi:10.1029/2022JA030288

Gasperini F, Forbes JM, Doornbos EN, Bruinsma SL (2015), Wave coupling between the lower and middle thermosphere as viewed from TIMED and GOCE, J Geophys Res 120:5788-05804, doi:10. 1002/2015JA021300

Gasperini F, Hagan ME, Zhao Y (2017), Evidence of tropospheric 90-day oscillations in the thermosphere, Geophys Res Lett., doi:10.1002/2017GL075445

Gasperini F, Forbes JM, Doornbos EN, Bruinsma SL (2018), Kelvin wave coupling from TIMED and GOCE: inter/intra-annual variability and solar activity effects, J Atmos Sol-Terr Phys 171, 176-187, doi:10.1016/j.jastp.2017.08.034

Gasperini F, Liu H, McInerney J (2020), Preliminary evidence of Madden-Julian oscillation effects on ultra- fast tropical waves in the thermosphere. J Geophys Res 125, doi:10.1029/ 2019JA027649

Gasperini F, Azeem I, Crowley G, Perdue M, Depew M, Immel T et al. (2021), Dynamical coupling between the low-latitude lower thermosphere and ionosphere via the non-migrating diurnal tide as revealed by concurrent satellite observations and numerical modeling, Geophys Res Lett, 48, doi:10.1029/2021GL093277

Goncharenko, L., Zhang, S.R. (2008), Ionospheric signatures of sudden stratospheric warming: Ion temperature at middle latitude, Geophys. Res. Lett., 35, L21103.

Goncharenko, L.P., Chau, J.L., Liu, H.L., Coster, A.J. (2010), Unexpected connections between the stratosphere and ionosphere, Geophys. Res. Lett., 37, L10101.

Goncharenko LP, Coster AJ, Plumb RA, Domeisen DIV (2012), The potential role of stratospheric ozone in the stratosphere-ionosphere coupling during stratospheric warmings, Geophys Res Lett 39, doi:10.1029/2012GL051261

Goncharenko, L. P., Harvey, V. L., Randall, C. E., Coster, A. J., Zhang, S.-R., Zalizovski, A., et al. (2022), Observations of Pole-to-Pole, stratosphere-to-ionosphere connection, Front. Astron. Space Sci. 8, doi:10.3389/fspas.2021.768629

Harding, B. J., Chau, J. L., He, M., Englert, C. R., Harlander, J. M., Marr, K. D., et al. (2021), Validation of ICON-MIGHTI thermospheric wind observations: 2. Green-line comparisons to specular meteor radars. Journal of Geophysical Research: Space Physics, 126(3), 1-12, doi:10.1029/2020JA028947

Harding, B. J., Makela, J. J., Englert, C. R., Marr, K. D., Harlander, J. M., England, S. L., and Immel, T. J. (2017), The MIGHTI wind retrieval algorithm: Description and verification. Space Science Reviews, 212(1–2), 585-600, doi:10.1007/s11214-017-0359-3

Harlander, J. M., Englert, C. R., Brown, C. M., Marr, K. D., Miller, I. J., Zastera, V., et al., (2017), Michelson Interferometer for Global High-Resolution Thermospheric Imaging (MIGHTI): Monolithic Interferometer Design and Test, Space Science Reviews, 212(1-2), 601-613, doi:10.1007/s11214-017-0358-4

Immel, T. J., England, S. L., Mende, S. B., Heelis, R. A., Englert, C. R., Edelstein, J., et al. (2018), The ionospheric connection explorer mission: Mission goals and design, Space Science Reviews, 214(1), 13, doi:10.1007/s11214-017-0449-2

Immel TJ, Eastes RW (2019), New NASA missions focus on terrestrial forcing of the space environment, Bull Am Meteorol Soc 100:2153-2156, doi:10.1175/BAMS-D-19-0066.1

Immel TJ, Harding BJ, Heelis RA, Maute A, Forbes JM, England SL et al. (2021), Regulation of ionospheric plasma velocities by thermospheric winds, Nat Geosci 14:893-898, doi:10.1038/s41561-021-00848-4

Jin, H., Miyoshi, Y., Pancheva, D., Mukhtarov, P., Fujiwara, H., and Shinagawa, H. (2012), Response of migrating tides to the stratospheric sudden warming in 2009 and their effects on the ionosphere studied by a whole atmosphere-ionosphere model GAIA with COSMIC and TIMED/ SABER observations, Journal of Geophysical Research, 117, A10323, doi:10.1029/2012JA017650

Jones, M. Jr., Siskind, D. E., Drob, D. P., McCormack, J. P., Emmert, J. T., Dhadly, M. S., et al. (2020), Coupling from the middle atmosphere to the exobase: Dynamical disturbance effects on light chemical species, Journal of Geophysical Research: Space Physics, 125, doi:10.1029/2020JA028331

Laskar, F. I., McCormack, J. P., Chau, J. L., Pallamraju, D., Hoffmann, P., and Singh, R. P. (2019), Interhemispheric meridional circulation during sudden stratospheric warming. Journal of Geophysical Research: Space Physics, 124,

7112-7122, doi:10.1029/2018JA026424

Lieberman, R. S., France, J., Ortland, D. A., and Eckermann, S. D. (2021), The role of inertial instability in cross-hemispheric coupling. Journal of the Atmospheric Sciences, 78(4), 1113– 1127, doi:10.1175/JAS-D-20-0119.1

Liu, H. L. (2017), Gravity Wave Variation from the Troposphere to the Lower Thermosphere during a Stratospheric Sudden Warming Event: A Case Study, SOLA, 13 (Special Edition), 24-30.

Liu, H.-L., and R. G. Roble (2002), A study of a self-generated stratospheric sudden warming and its mesospheric/lower thermospheric impacts using coupled TIME-GCM/CCM3, J. Geophys. Res., 107, doi:10.1029/2001JD001533.

Liu, H.-L., Wang, W., Richmond, A. D., and Roble, R. G. (2010), Ionospheric variability due to planetary waves and tides for solar minimum conditions. Journal of Geophysical Research, 115, A00G01, doi:10.1029/2009ja015188

Liu, H., H. Jin, Y. Miyoshi, H. Fujiwara, and H. Shinagawa (2013), Upper atmosphere response to stratosphere sudden warming: Local time and height dependence simulated by gaia model. Geophys. Res. Lett., 40, 635-640, doi:10.1002/grl.50146.

Liu, H., Y. Miyoshi, S. Miyahara, H. Jin, H. Fujiwara, and H. Shinagawa (2014), Thermal and dynamical changes of the zonal mean state of the thermosphere during the 2009 SSW: Gaia simulations. J. Geophys. Res.: Space Phys., 119, 6784-6791, doi:10.1002/2014JA020222.

Liu, J., Zhang, D., Sun, S., Hao, Y., and Xiao, Z. (2022), Ionospheric semi-diurnal lunitidal perturbations during the 2021 Sudden Stratospheric Warming event: Latitudinal and inter-hemispheric variations in the American, Asian-Australian, and African-European sectors. Journal of Geophysical Research: Space Physics, e2022JA030313.

Liu, G., England, S. L., Immel, T. J., Kumar, K. K., Ramkumar, G., & Goncharenko, L. P. (2012), Signatures of the 3-day wave in the low-latitude and midlatitude ionosphere during the January 2010 URSI World Day campaign. Journal of Geophysical Research, 117, A06305, doi:10.1029/2012JA017588

Liu, G., Janches, D., Ma, J., Lieberman, R. S., Stober, G., Moffat-Griffin, T., et al. (2022), Mesosphere and lower thermosphere winds and tidal variations during the 2019 Antarctic Sudden Stratospheric Warming. Journal of Geophysical

Research: Space Physics, 127, e2021JA030177, doi:10.1029/2021JA030177

Lu, Q., Rao, J., Liang, Z., Guo, D., Luo, J., Liu, S., et al. (2021), The sudden stratospheric warming in January 2021, Environmental Research Letters, 16(8), 084029.

Makela, J. J., Baughman, M., Navarro, L. A., Harding, B. J., Englert, C. R., Harlander, J. M., et al. (2021), Validation of ICON-MIGHTI thermospheric wind observations: 1. Nighttime red-line ground-based Fabry-Perot interferometers, Journal of Geophysical Research: Space Physics, 126(2), 1-29, doi:10.1029/2020JA028726.

Matsuno, T. A Dynamical Model of the Stratospheric Sudden Warming. J. Atmos. Sci. 1971, 28, 1479-1494.

Miyoshi, Y., H. Fujiwara, H. Jin, and H. Shinagawa (2015), Impacts of sudden stratospheric warming on general circulation of the thermosphere, J. Geophys. Res. Space Phys., 120, 10897-10912, 2015JA021894.

Oberheide, J., Pedatella, N. M., Gan, Q., Kumari, K., Burns, A. G., and Eastes, R. W. (2020), Thermospheric composition O/N2 response to an altered meridional mean circulation during Sudden Stratospheric Warmings observed by GOLD, Geophysical Research Letters, 47(1), doi:10.1029/2019GL086313

Oberheide, J. (2022), Day-to-day variability of the semidiurnal tide in the F-region ionosphere during the January 2021 SSW from COSMIC-2 and ICON, Geophysical Research Letters, 49, doi:10.1029/2022GL100369

Orsolini, Y. J., Zhang, J., and Limpasuvan, V. (2022), Abrupt Change in the Lower Thermospheric Mean Meridional Circulation during Sudden Stratospheric Warmings and its Impact on Trace Species, Journal of Geophysical Research: Atmospheres, doi:10.1029/2022JD037050

Pancheva, D., Mukhtarov, P., and Andonov, B. (2009), Nonmigrating tidal activity related to the sudden stratospheric warming in the Arctic winter of 2003/2004, Annales Geophysicae, 27, 975-987, doi:10.5194/angeo-27-975-2009

Pedatella, N. M., and Liu, H.-L. (2013), The influence of atmospheric tide and planetary wave variability during sudden stratosphere warmings on the low latitude ionosphere. Journal of Geophysical Research, 118, 5333-5347, doi:10.1002/jgra.50492

Pedatella, N. M., Liu, H.-L., Richmond, A. D., Maute, A., and Fang, T.-W. (2012), Simulations of solar and lunar tidal variability in the mesosphere and lower thermosphere during sudden stratosphere warmings and their influence on the low-latitude ionosphere, Journal of Geophysical Research, 117, A08326, doi:10.1029/2012ja017858

Pedatella, N., Liu, H. L., Sassi, F., Lei, J., Chau, J., and Zhang, X. (2014), Ionosphere variability during the 2009 SSW: Influence of the lunar semidiurnal tide and mechanisms producing electron density variability. Journal of Geophysical Research: Space Physics, 119, 3828-3843, doi:10.1002/2014ja019849

Pedatella, N.-M., Fang, T. W., Jin, H., Sassi, F., Schmidt, H., Chau, J.-L., et al. (2016), Multimodel comparison of the ionosphere variability during the 2009 sudden stratosphere warming. Journal of Geophysical Research: Space Physics, 121, 7204-7225, doi:10.1002/ 2016ja022859

Pedatella, N.M., Chau, J.L., Schmidt, H., Goncharenko, L.P., Stolle, C., Hocke, K., Harvey, V.L., Funke, B., Siddiqui, T.A (2018), How sudden stratospheric warming affects the whole atmosphere, EOS, 99, 35-38.

Pedatella, N. (2022), Ionospheric variability during the 2020-2021 SSW: COSMIC-2 observations and WACCM-X simulations, Atmosphere, 13(3), 368, doi:10.3390/atmos13030368

Phanikumar, D., Kumar, K. N., & Kumar, S. (2014), Signatures of ultra-fast Kelvin waves in low latitude ionospheric TEC during January 2009 stratospheric warming event, Journal of Atmospheric and Solar-Terrestrial Physics, 117, 48-53.

Rao, J., Garfinkel, C. I., Wu, T., Lu, Y., Lu, Q., and Liang, Z. (2021), The January 2021 sudden stratospheric warming and its prediction in subseasonal to seasonal models, Journal of Geophysical Research: Atmospheres, 126, doi:10.1029/2021JD035057

Sassi, F., Liu, H. L., Ma, J., & Garcia, R. R. (2013), The lower thermosphere during the Northern Hemisphere winter of 2009: A modeling study using high-altitude data assimilation products in WACCM-X, Journal of Geophysical Research: Atmospheres, 118, 8954-8968.

Sathishkumar, S., and Sridharan, S. (2013), Lunar and solar tidal variabilities in mesospheric winds and EEJ strength over Tirunelveli (8.7N, 77.8E) during the

494 2009 major stratospheric warming, Journal of Geophysical Research: Space
495 Physics, 118(1), 533-541, doi:10.1029/2012JA018236

496 Siddiqui TA, Maute A, Pedatella NM (2019), On the importance of interactive ozone
497 chemistry in Earth-System models for studying mesophere-lower thermosphere
498 tidal changes during sudden stratospheric warmings, J Geophys Res Space
499 Phys 124(12), 10690-10707, doi:10.1029/2019JA027193

500 Siddiqui, T. A., Chau, J. L., Stolle, C., and Yamazaki, Y. (2022), Migrating solar
501 diurnal tidal variability during Northern and Southern Hemisphere Sudden
502 Stratospheric Warmings, Earth, Planets and Space, 74(1), 1-17.

503 Stening, R.J. (1977), Electron density profile changes associated with the equatorial
504 electrojet, J. Atmos. Terr. Phys., 39, 157-164.

505 Tan, B., X. Chu, H.-L. Liu, C. Yamashita, and J. M. R. III (2012), Zonal-mean
506 global teleconnection from 15 to 110 km derived from saber and waccm, J.
507 Geophys. Res., doi:10.1029/ 2011JD016750.

508 Wang, J. C., Yue, J., Wang, W., Qian, L., Wu, Q., and Wang, N. (2022), The
509 lower thermospheric winter-to-summer meridional circulation: 1. Driv-
510 ing mechanism, Journal of Geophysical Research: Space Physics, 127,
511 doi:10.1029/2022JA030948

512 Yamazaki, Y., Miyoshi, Y., Xiong, C., Stolle, C., Soares, G., and Yoshikawa, A.
513 (2020), Whole atmosphere model simulations of ultra-fast Kelvin wave effects
514 in the ionosphere and thermosphere. Journal of Geophysical Research: Space
515 Physics, 125, doi:10.1029/2020JA027939

516 Yiğit, E., and Medvedev, A. S. (2012), Gravity waves in the thermosphere during a
517 sudden stratospheric warming, Geophysical Research Letters, 39, L21101.

518 Yiğit, E., and Medvedev, A. S. (2016), Role of gravity waves in vertical cou-
519 pling during sudden stratospheric warmings, Geoscience Letters, 3, 27,
520 doi:10.1186/s40562-016-0056-1

521 Yiğit, E., Medvedev, A. S., England, S. L., and Immel, T. J. (2014), Simulated vari-
522 ability of the high-latitude thermosphere induced by small-scale gravity waves
523 during a sudden stratospheric warming, Journal of Geophysical Research:
524 Space Physics, 119, 357-365.

525 Yiğit, E., P. K. Knížová, K. Georgieva, and W. Ward (2016), A review of vertical
526 coupling in the atmosphere-ionosphere system: Effects of waves, sudden strato-

spheric warmings, space weather, and of solar activity, J. Atmos. Sol. Terr. Phys., 141, 1-12, doi:10.1016/j.jastp.2016.02.011.

Yiğit, E., Dhadly, M., Medvedev, A. S., Harding, B. J., Englert, C. R., Wu, Q., and Immel, T. J. (2022), Characterization of the Thermospheric Mean Winds and Circulation during Solstice using ICON/MIGHTI Observations, Journal of Geophysical Research: Space Physics, 127, doi:10.1029/2022JA030851

Yuan, T., B. Thurairajah, C.-Y. She, A. Chandran, R. L. Collins, and D. A. Krueger (2012), Wind and temperature response of midlatitude mesopause region to the 2009 sudden stratospheric warming, J. Geophys. Res., 117, D09114, doi:10.1029/2011JD017142

Zhang, J., Limpasuvan, V., Orsolini, Y. J., Espy, P. J., and Hibbins, R. E. (2021), Climatological westward-propagating semidiurnal tides and their composite response to sudden stratospheric warmings in SuperDARN and SD-WACCM-X, J. Geophys. Res. Atm., 126, doi:10.1029/2020JD032895

Zhang, J., Y. Orsolini, V. Limpasuvan (2022), Abrupt Change in the Lower Thermospheric Mean Meridional Circulation during Sudden Stratospheric Warmings and its Impact on Trace Species, CEDAR Workshop MLT Poster, https://cedarscience.org/poster-2022/abrupt-change-lower-thermospheric-mean-meridional-circulation-during-sudden

Zhang, R., Liu, L., Ma, H., Chen, Y., and Le, H. (2022), ICON observations of equatorial ionospheric vertical ExB and field-aligned plasma drifts during the 2020-2021 SSW. Geophysical Research Letters, 49, e2022GL099238, doi:10.1029/2022GL099238

Zulicke, C., Becker, E., Matthias, V., Peters, D.-H.-W., Schmidt, H., Liu, H. L., et al. (2018), Coolings in observations and simulations coupling of stratospheric warmings with mesospheric coolings in observations and simulations. Journal of Climate, 31(3), 1107-1133, doi:10.1175/jcli-d-17-0047.1

Figure 1.

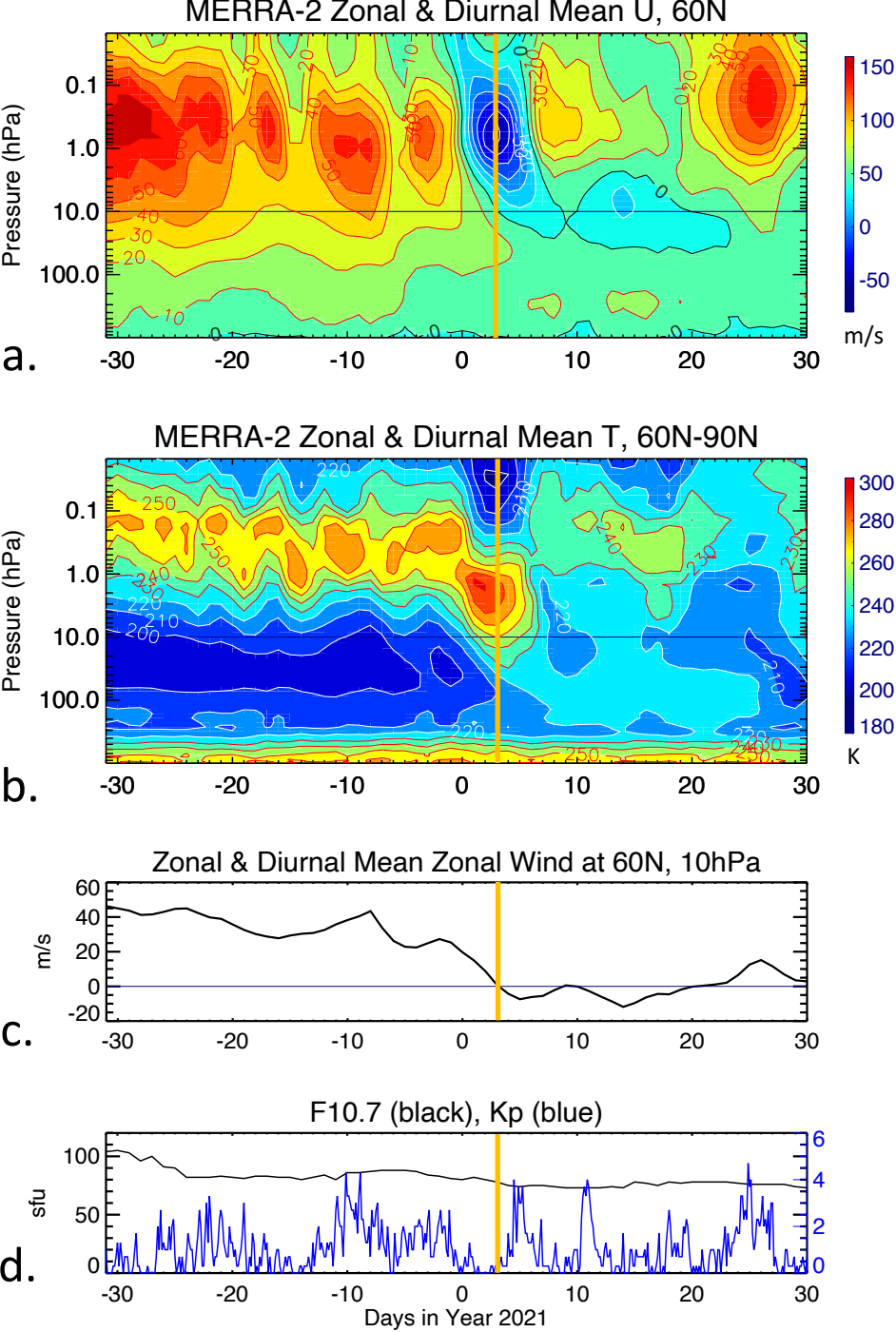
MERRA-2 Zonal & Diurnal Mean U, 60N
Pressure (hPa)
0.1
1.0
10.0
100.0
-30
-20
-10
0
10
20
30
150
100
50
0
-50
m/s
a.
MERRA-2 Zonal & Diurnal Mean T, 60N-90N
Pressure (hPa)
300
280
260
240
220
200
180
K
b.
Zonal & Diurnal Mean Zonal Wind at 60N, 10hPa
m/s
60
40
20
0
-20
c.
F10.7 (black), Kp (blue)
sfu
100
50
0
6
4
2
0
d.
Days in Year 2021

Figure 2.

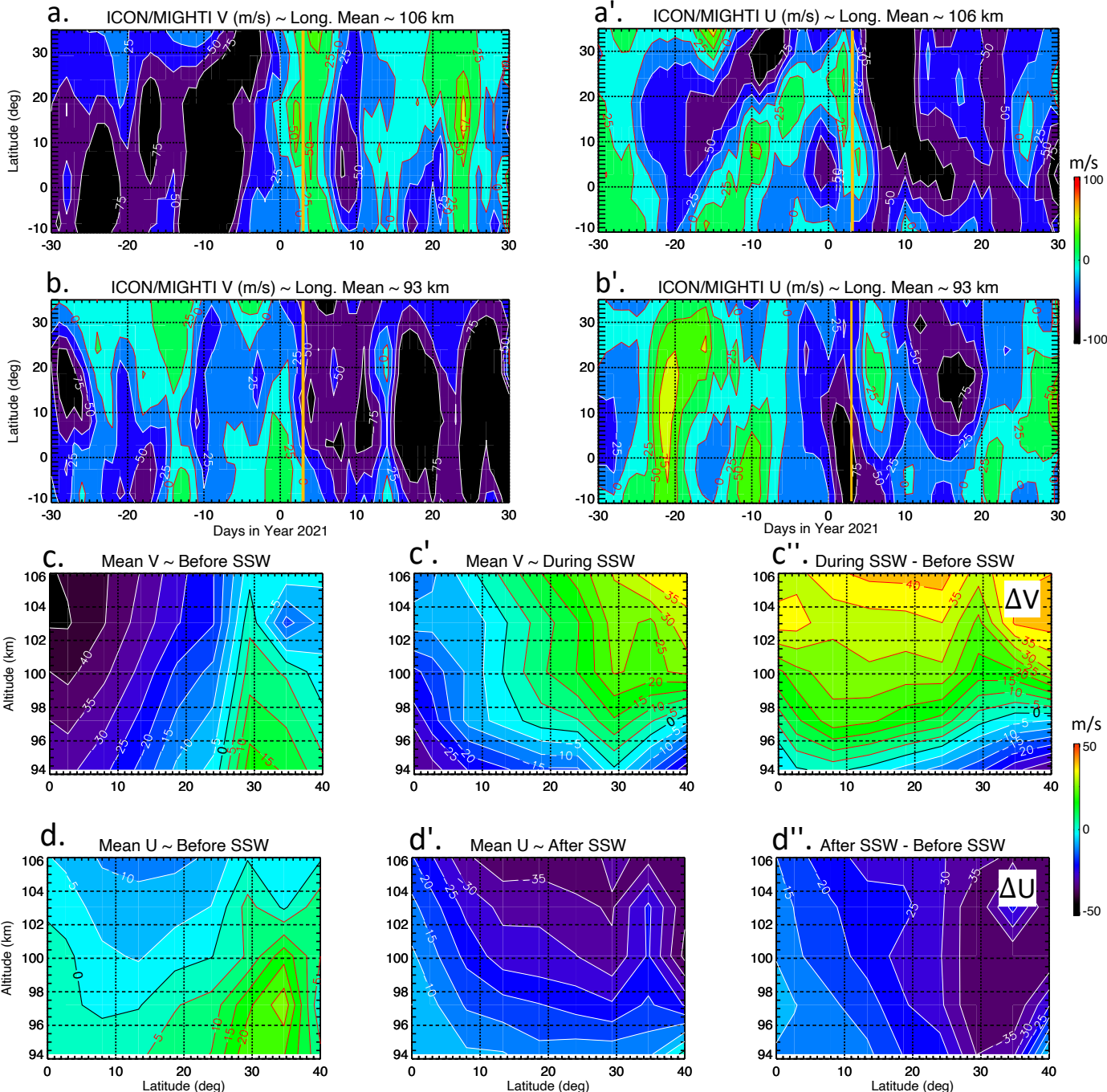
a.
ICON/MIGHTI V (m/s) ~ Long. Mean ~ 106 km
a'.
ICON/MIGHTI U (m/s) ~ Long. Mean ~ 106 km
b.
ICON/MIGHTI V (m/s) ~ Long. Mean ~ 93 km
b'.
ICON/MIGHTI U (m/s) ~ Long. Mean ~ 93 km
Latitude (deg)
Days in Year 2021
m/s
100
0
-100
c.
Mean V ~ Before SSW
c'.
Mean V ~ During SSW
c''.
During SSW - Before SSW
ΔV
d.
Mean U ~ Before SSW
d'.
Mean U ~ After SSW
d''.
After SSW - Before SSW
ΔU
Altitude (km)
Latitude (deg)
50
-50

Figure 3.

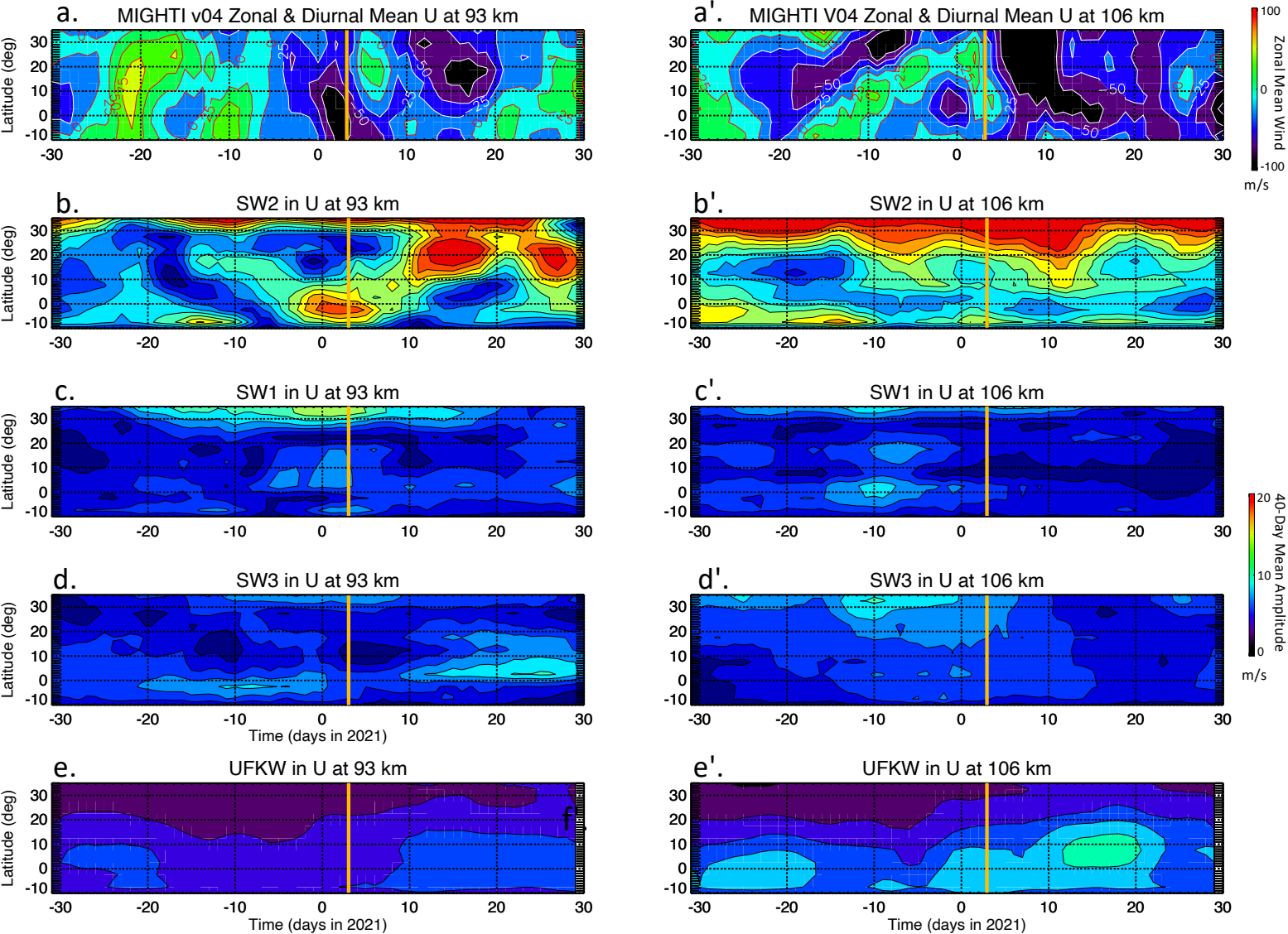
a.
MIGHTI v04 Zonal & Diurnal Mean U at 93 km
a'.
MIGHTI V04 Zonal & Diurnal Mean U at 106 km
Zonal Mean Wind
m/s
b.
SW2 in U at 93 km
b'.
SW2 in U at 106 km
c.
SW1 in U at 93 km
c'.
SW1 in U at 106 km
d.
SW3 in U at 93 km
d'.
SW3 in U at 106 km
40-Day Mean Amplitude
m/s
e.
UFKW in U at 93 km
e'.
UFKW in U at 106 km
Latitude (deg)
Time (days in 2021)